Opto-Electronic Advances

Perspective

December 2025, Vol. 8, No. 12

DOI: 10.29026/oea.2025.250256 CSTR: 32247.14.oea.2025.250256

Surpassing the diffraction limit in long-range laser engineering via cross-scale vectorial optical field manipulation: perspectives and outlooks

Yinghui Guo[1,2,3], Mingbo Pu[1,2,3]*, Yang Li[1,2,3], Mingfeng Xu[1,2,3] and Xiangang Luo[1,2,3]*

We present a vectorial optical field (VOF) framework that surpasses the diffraction limit in both long-range imaging and energy delivery. By jointly engineering spatial and temporal dimensions, reflective Fourier ptychography is extended to 3.2 km with 0.37× the classical diffraction limit, while a single-photon LiDAR tomography system achieves centimeter-scale, sub-diffraction imaging at 3.3 km using superconducting nanowire single-photon detectors. These advances demonstrate super-resolution, turbulence-resilient imaging over kilometer-range distances. Beyond super-resolution optical, high power VOFs are able to counteract thermal blooming during atmospheric laser propagation, enhancing on-target power density by a factor larger than 2. Together, these results may outline a cross-scale paradigm that links high-power vector-field structuring, single-photon detection, and adaptive control—offering a pathway toward next-generation optical systems that integrate imaging, sensing, communication and directed energy within a common physical framework.

Keywords: generalized diffraction limit; cross-scale vectorial optical field manipulation; sub-diffraction-limited imaging; laser wireless power transfer; laser-induced atmosphere engineering

Guo YH, Pu MB, Li Y et al. Surpassing the diffraction limit in long-range laser engineering via cross-scale vectorial optical field manipulation: perspectives and outlooks. *Opto-Electron Adv* **8**, 250256 (2025).

Introduction

The optical diffraction limit remains one of the most fundamental challenges in optics and photonics. Among the 125 Frontier scientific questions released by *Science* in 2021, the question "Is there a diffraction limit?" ranked first in physics—highlighting the scientific community's long-standing urgency to address this question amid the pursuit of ideal optical devices and systems. Historically, the diffraction limit was solely regarded as the minimum resolution of optical imaging, first defined by Abbe and Rayleigh in the 1870s. Recently, it has become clear that numerous other optical performances metrics—such as the depth of focus limit, and power density limit—are also fundamentally constrained by light's diffractive nature.

[1]State Key Laboratory of Optical Field Manipulation Science and Technology, Institute of Optics and Electronics, Chinese Academy of Sciences, Chengdu 610209, China; [2]Research Center on Vector Optical Fields, Institute of Optics and Electronics, Chinese Academy of Sciences, Chengdu 610209, China; [3]College of Materials Sciences and Opto-Electronic Technology, University of Chinese Academy of Sciences, Beijing 100049, China.

*Correspondence: MB Pu, E-mail: pmb@ioe.ac.cn; XG Luo, E-mail: lxg@ioe.ac.cn

Received: 24 September 2025; Accepted: 4 November 2025; Published online: 25 December 2025

Open Access This article is licensed under a Creative Commons Attribution 4.0 International License.
To view a copy of this license, visit http://creativecommons.org/licenses/by/4.0/.

© The Author(s) 2025. Published by Institute of Optics and Electronics, Chinese Academy of Sciences.

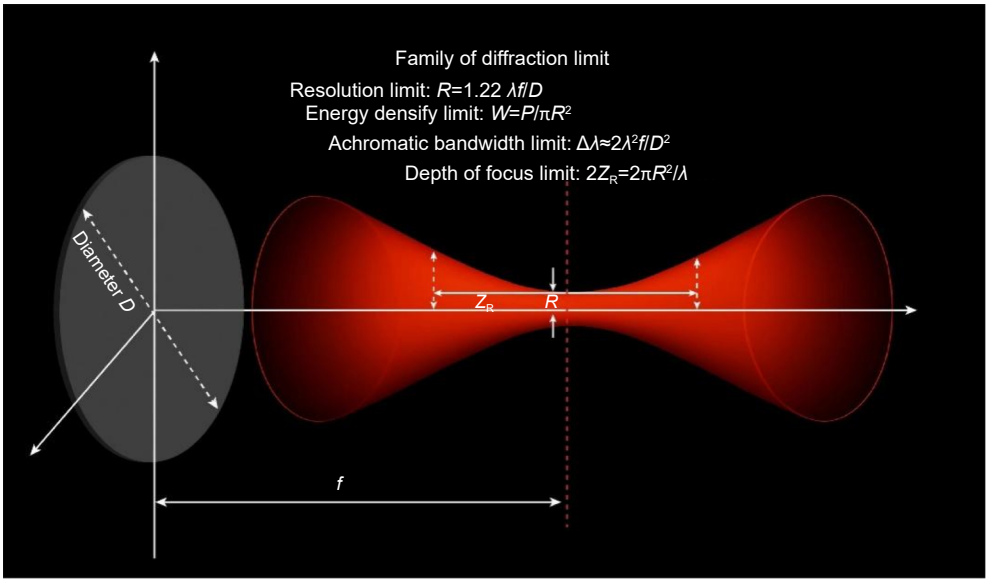

Fig. 1 | Family of diffraction limit encompassing resolution limit, energy density limit, achromatic bandwidth limit, depth of focus limit and other related constraints.

Collectively, these restrictions can be referred to as the *generalized diffraction limit* or *family of the diffraction limit*[1,2], as illustrated in Fig. 1.

Since the turn of the 21st century, breakthroughs in plasmonics, metamaterials, and metasurfaces have enabled optical engineering to extend deep into the subwavelength regime, uncovering a suite of anomalous optical phenomena—including Wood's anomaly, extraordinary optical transmission (EOT)[3], and extraordinary Young's interference (EYI)[4]. These discoveries have highlighted the critical roles of near-field vectorial optical coupling, evanescent-to-propagating wave conversion, and localized phase-shift manipulation in optics engineering, representing novel effects that classical scalar optics cannot predict or exploit[5–8]. Coupled with the full control of amplitude, phase, dispersion, and polarization[9–23] —achieved with unprecedented flexibility in both spatial and temporal domains—optical research has entered the era of Vectorial Optics.

As indicated in Fig. 2, Vectorial Optics exhibits at least two particularly notable features: First, the generalized laws of reflection and refraction—based on local gradient phase modulation—break the constraints of classical optical reflection and refraction laws[5,24,25]. This enables the transition of optical devices from curved to planar architectures[26,27], rendering them more lightweight and amenable to mass production. For instance, wide-field-of-view (WFOV) cameras —traditionally composed of multiple bulky lenses —can instead be realized using a monolithic flat metalens with a quadratic-phase profile[28–30]. Meahwhile, cascaded metasurfaces can be harnessed to enhance polarization multiplexing capability, enable rapid broadband polarization modulation, and achieve dynamic optical field manipulation. Second, the manipulation and utilization of high-spatial-frequency evanescent waves—enabled by local gradient phase modulation—overcome the optical diffraction limit, enabling higher imaging resolution and smaller focused light spots. For example, sub-diffraction-limited imaging has been demonstrated using artificially designed superlenses[31,32], hyperlens[33], superoscillatory lens[34] and tight focusing characteristics of VOFs[35]. In superlenses and hyperlenses, vectorial modes (e.g., surface plasmon polaritons) can be excited in the near field, with wavevectors exceeding those of free-space light—enabling super-resolution imaging beyond the diffraction limit[36]. Similarly, the laser-induced lensing effect could be utilized to realize a smaller focusing spot, and correspondingly a higher power density[37].

Despite these breakthroughs, most advancements in VOF-based systems have been largely restricted to short-range and linear regimes[38]. For long-range free-space optical (FSO) applications —including remote imaging, laser wireless power transfer (LWPT), LiDAR, and laser

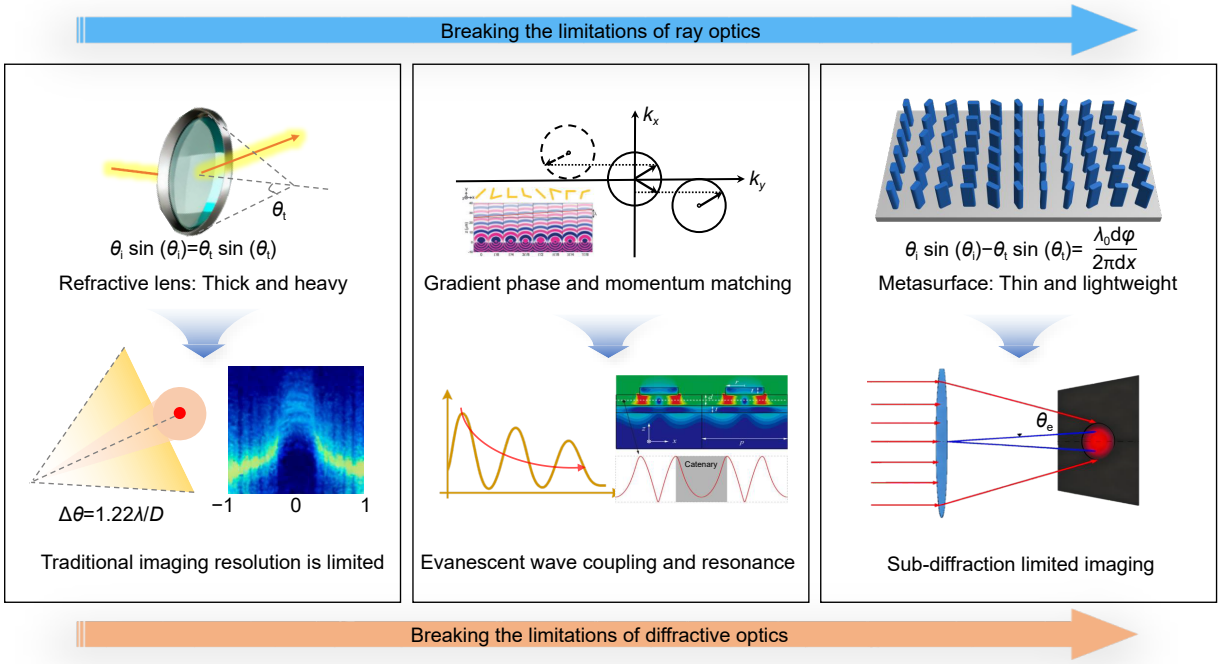

Fig. 2 | Two defining features of Vectorial Optics imaging: breaking classical reflection/refraction laws and the diffraction limit via local, abrupt phase or wavevector manipulation. Figure reproduced with permission from: ref.[4], American Chemical Society; ref.[10], under a Creative Commons Attribution 4.0 International License; ref.[24], Optical Society of America.

communication—conventional optical systems are typically designed and optimized for clear atmospheric conditions. However, terrestrial FSO links are inherently limited by weather, imposing severe constraints on efforts to approach the diffraction limit. For example, atmospheric turbulence and scattering—coupled with diffuse target reflection—distort wavefronts and degrade spatial coherence, complicating the implementation of synthetic aperture techniques. Furthermore, high-power laser propagation is strongly affected by atmosphere turbulence and nonlinear thermal blooming effects that increase beam divergence, induce intensity scintillation, and reduce on-target peak irradiance (power density)[39]. Beyond a critical threshold, simply increasing aperture size or laser power does not yield proportional improvements in far-field energy delivery. A key question thus arises: Can the superior characteristics of VOFs be harnessed in long-range, high-power applications to achieve enhanced resolution and energy density? Addressing this challenge demands large-scale platforms for VOF manipulation. In this context, we present two representative demonstrations illustrating how cross-scale VOF manipulation can surpass diffraction limits for both information and energy transfer.

Surpassing the long-range diffraction limit of light

Information transfer: long-range laser active imaging

Optical synthetic apertures (OSAs) represent a well-established approach for improving imaging resolution. However, in passive imaging systems (which rely on ambient light or target self-radiation), multiple sub-mirrors demand strict co-phasing (typically < $\lambda/20$)—a requirement that presents significant challenges for the fabrication and assembly of optical telescopes, especially for large-scale remote sensing platforms. In contrast, macroscopic Fourier ptychography (FP) imaging, as a typical form of active imaging, could circumvent this limitation: by aperture scanning to acquire multi-position diffraction patterns of the target, and integrating phase retrieval algorithms with OSAs imaging principles. FP achieves sub-diffraction resolution without strict co-phasing constraints[40–42], which can operates across multiple wavelength regimes, from electron (picometres) to X-ray (~0.1 nm), extreme ultraviolet (~10 nm) and visible light (micrometers)[43]. This active imaging nature of FP not only reduces dependence on external light

Table 1 | Comparison of typical macroscopic FP sub-diffraction limited imaging.

Year	Institute	Imaging distance (m)	Single aperture size (mm)	Equivalent synthetic aperture size
2014	UConn	0.7	2.5	2.5 mm×4[45]
2016	Rice University	1.5	2.3	2.3 mm×7[46]
2017	Rice University	1	2.3	2.3 mm×6[47]
2023	NJUST	12	2.3	2.3 mm×8[48]
2023	DMU	10	5.2	5.2 mm×6[49]
2023	IOE, CAS	120	50	50 mm×4[44]
2024	IOE, CAS	1.4 km	100	100 mm×2.5
2025	IOE, CAS	3.2 km	300	300 mm×2.7

conditions but also enables flexible manipulation of the imaging information dimension, making it particularly suitable for scenarios where passive imaging struggles (such as low-light remote sensing or opaque target imaging). Although FP exhibits great potential for improving the imaging resolution of remote sensing systems, previous experimental demonstrations have been largely restricted to laboratory-scale distances (~10 m)—a gap that needs to be addressed for its practical application in long-range remote sensing, as summarized in Table 1.

Since 2023, our group has extended reflective FP imaging to unprecedented scales: 120 m with a 50 mm aperture[44], 1.4 kilometers (single aperture size D = 100 mm) in 2024, and 3.2 kilometers (single aperture size D

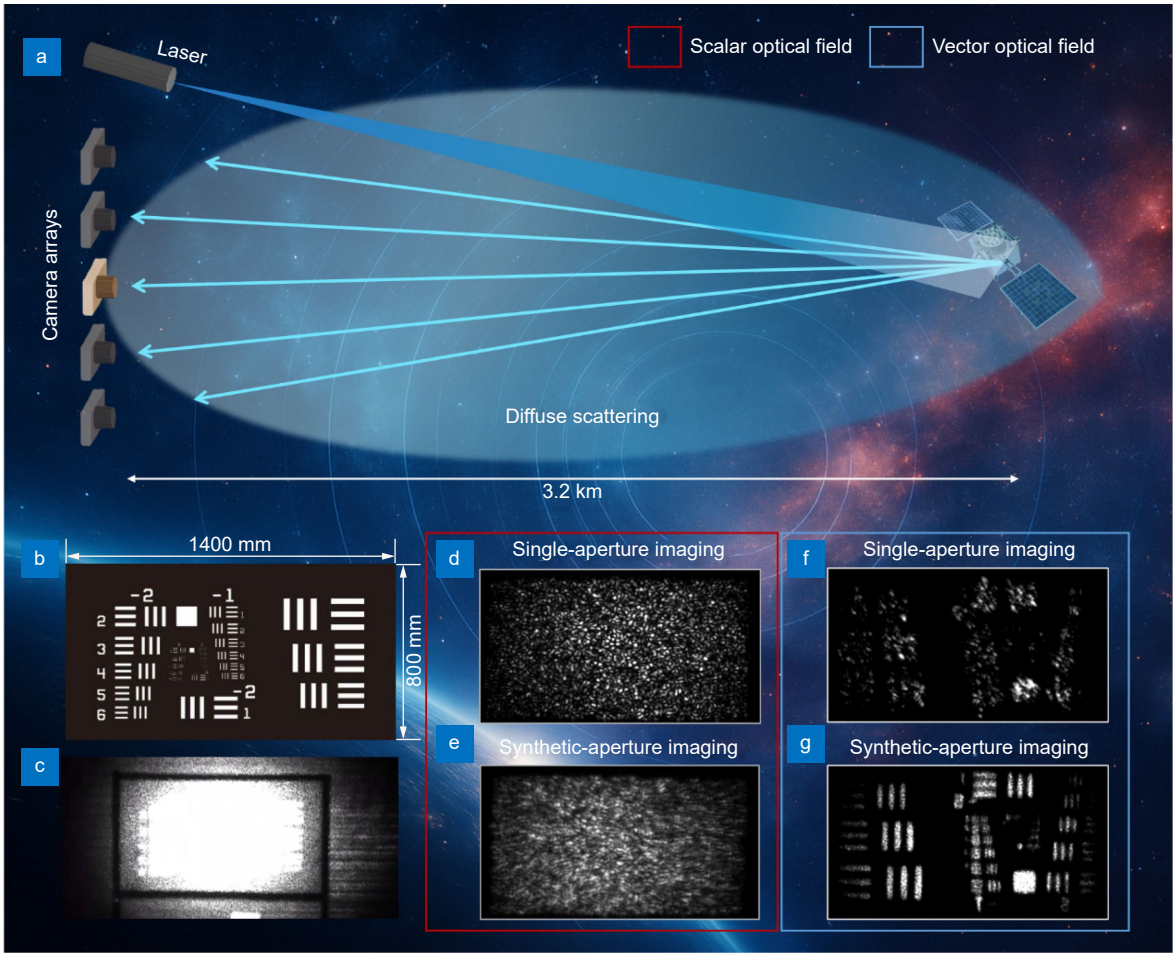

Fig. 3 | Surpassing the information diffraction limit at the kilometer-scale via macroscopic FP imaging. (**a**) Schematic of 3.2 km reflective FP imaging. (**b**) Ground-truth image of the resolution target. (**c**) Image of the resolution target under coherent illumination by a 50 W 1064 nm laser, captured at 20 m using an infrared camera (Goldeye G-130 TEC1). (**d**) Single-aperture and (**e**) synthetic aperture imaging without orthogonal polarization filtering. (**f**) Single-aperture and (**g**) synthetic aperture imaging with orthogonal polarization filtering.

= 300 mm, as illustrated in Fig. 1) in 2025. Figure 3(a) presents the schematic and hardware layout of our kilometer-scale FP system, which was implemented in an environmentally controlled 3.2 km-long underground tunnel. The typical environmental conditions in the underground tunnel are provided in Table S1 and Fig. S1. A custom resolution target—shown in Fig. 3(b), with its geometry specified in Table S2—is placed at the tunnel terminus and illuminated by a high-power 1064 nm laser. The backscattered light is collected at the opposite end using a 300 mm-aperture Cassegrain telescope, as showing in Fig. S2. To ensure sufficient imaging contrast at 3.2 km, the laser output power was set to 50 W, resulting in an overexposed image captured at 20 m (Fig. 3(c)). The 300 mm-aperture telescope is mounted on a long-stroke, high-precision two-axis translation stage (X and Z travel: 1.5 m each; positioning accuracy < 3 μm). We acquired 625 (25 × 25) short-exposure frames (30 ms per frame) by translating the telescope in 52.5 mm steps (corresponding to an 82.5% overlap).

Due to the high coherence of the laser source, strong laser speckle is mixed with specular reflection—obscuring the retrieval of weak high-frequency spatial information from the reflective target (Fig. 3(d)). Consequently, the resolution target remained unresolvable (Fig. 3(e)) —even when using an FP-based optical synthetic aperture. We further observed that the polarizations of specular and diffuse reflection are nearly mutually orthogonal. Leveraging this property, we fully accounted for and exploited the vectorial nature of the total reflected light. As shown in Fig. 3(f), imaging contrast was significantly improved after polarization filtering. Although some laser speckle persisted, it was significantly suppressed using the FP-based optical synthetic aperture (Fig. 3(g)). Using a contrast ratio as the evaluation criterion (defined in ref.[47] but with a higher threshold of 0.15 here), the period of the smallest resolvable line pair was measured to be 11.2 mm—~0.37× the optical diffraction limit (corresponding to a ~2.7× improvement relative to the coherent diffraction limit, defined as $2.44\lambda L/D$). These results clearly demonstrate that VOF manipulation can overcome the far-field diffraction limit in optical imaging. To address the prolonged aperture-scanning time, a camera array architecture can enable real-time FP imaging —even in a neural network-based manner[42].

Beyond macroscopic FP imaging, LiDAR tomography emerges as an advanced modality to overcome the inherent limitations of conventional LiDAR. Its core principle for high-resolution target reconstruction involves acquiring range profile images of unresolved targets across multiple aspect angles[50–53]. Unlike conventional optical systems—where resolution is tightly constrained by aperture size and target distance—LiDAR tomography's resolution depends solely on its depth resolution. Notably, it is no longer tied to the optical aperture, but dominated by two key factors including laser pulse width and detector temporal resolution. We thus term this mechanism "Imaging resolution conversion between spatiotemporal domain".

Here, we present a high-performance LiDAR tomography system that experimentally demonstrates single-photon imaging beyond the diffraction limit at a 3.3 km stand-off distance. By integrating time-correlated single-photon counting (TCSPC) with superconducting nanowire single-photon detectors (SNSPDs), the system attains sub-10 ps timing precision and exceptional temporal resolution.

In the receiver module, echo photons are coupled into the SNSPD through a single-mode fiber, which minimizes chromatic dispersion and functions as a spatial pinhole to suppress background noise. A fast-steering mirror ensures precise target tracking, while a 350 mm Cassegrain-RC telescope serves as the primary receiving aperture. On the transmission side, polarization filtering and conversion to vertical polarization via a half-wave plate effectively eliminate stray reflections.

The SNSPD operates at 2.2 K, providing <13 ps timing jitter and 88 % detection efficiency at 1550 nm. A synchronized laser trigger establishes accurate time correlation between the TCSPC module (2 ps bin width, 10 ps jitter) and a 7.2 ps pulsed laser source. Experiments were performed using a two-axis telescope platform to scan an 8 mm line-pair target. Operating in confocal mode improved the signal-to-noise ratio (SNR) by 4.8 dB, enabling fine reconstruction of target features.

Photon-count data were processed through projection registration, deconvolution-based denoising, and two-dimensional reconstruction using a filtered back-projection (FBP) algorithm. As shown in Fig. 4, the system achieved an 8 mm line-pair resolution at 3.3 km; the reconstructed image clearly resolves line pairs with >60% peak-to-valley contrast, confirming sub-diffraction performance and strong atmospheric robustness. These results validate the LiDAR tomography system's capability for all-weather, long-range, high-resolution imaging and

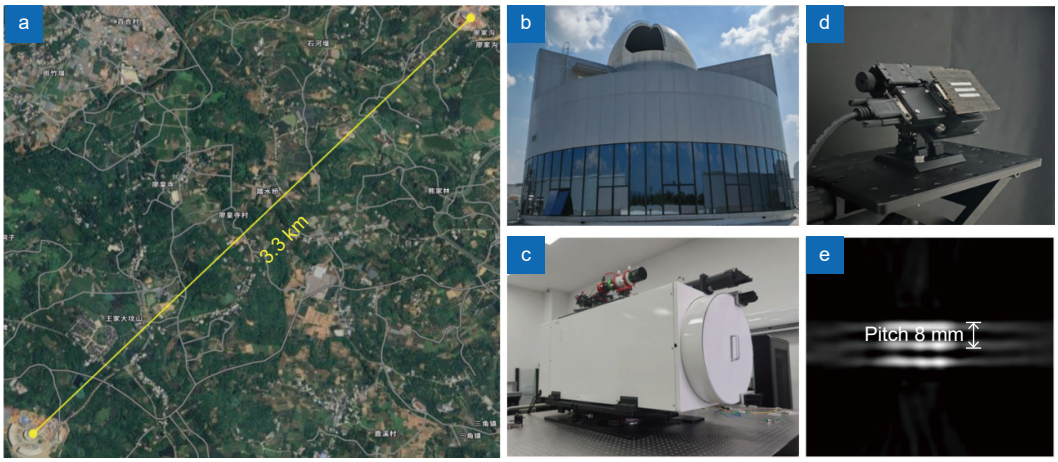

Fig. 4 | Surpassing the information diffraction limit at the kilometer scale via spatiotemporal resolution conversion in LiDAR tomography. (**a**) Satellite map of the 3.3 km imaging link; the LiDAR tomography experiment was conducted on 20 April 2025 at 15:00 in Chengdu, China. (**b**) Building at the terminus of the 3.3 km link. (**c**) 350 mm-aperture Cassegrain-RC telescope. (**d**) 8 mm-pitch line-pair imaging target mounted on a two-axis rotating stage. (**e**) Reconstructed imaging results.

highlight its strong potential for space-debris monitoring and satellite recognition applications.

Energy transfer: directed energy laser and LWPT

With the rapid development and deployment of unmanned aerial vehicles (UAVs) in fields including surveillance, disaster relief, and scientific exploration, the demand for prolonged flight endurance has grown increasingly urgent. One of the most promising solutions to this challenge is LWPT, which enables UAVs to be recharged or powered in real time without landing. In principle, LWPT establishes a direct optical link between a ground-based or airborne laser source and a photovoltaic/thermal receiver mounted on the UAV, converting laser radiation into usable electrical power. Under relatively low-power operation, the received energy scales nearly linearly with the laser output power. However, as transmitted power increases to the high-power regime, nonlinear atmospheric effects begin to dominate the propagation process. Among these effects, thermal blooming and self-focusing are particularly critical.

Thermal blooming originates from the non-uniform absorption of laser energy by atmospheric molecules, leading to localized heating and the formation of a refractive index gradient along the beam path. This gradient acts as a distributed "negative thermal lens", effectively defocusing the laser beam and causing it to diverge during propagation. This results in a substantial reduction in the power density delivered to the UAV target—illustrated by the blue curve in Fig. 5(a), where the expected linear scaling collapses due to severe thermal distortion.

A promising solution involves using high-power VOFs with non-Gaussian intensity profiles (e.g., cylindrical vector beams) as auxiliary heating sources. These beams generate "positive thermal lenses" that compensate for thermal blooming, counteracting the divergence induced by the negative thermal lens and correcting high-power beam distortion. To verify this hypothesis, numerical simulations of Gaussian laser beam propagation are presented in Fig. 5(b) and 5(c), where a vortex auxiliary laser—operating at a wavelength of strong atmospheric absorption and carrying only 0.35% of the Gaussian beam's power—is employed to induce an atmospheric lens. Simulated results with and without the auxiliary vector beam are shown in Fig. 5(b) and 5(c), respectively. One can observe that the maximum power density in the former case is 2.7× that of the latter. Thus, it is anticipated that power density will continue to increase in future applications through adaptive or even intelligent VOF engineering—as indicated by the red curve in Fig. 5(a).

For pulsed lasers with intensities above 1 GW/cm^2, self-focusing provides an additional pathway to surpass the energy diffraction limit, enabling faster energy transfer or laser material processing. Both numerical and experimental studies have shown that focused power densities can far exceed classical theoretical predictions[54–56]. Nevertheless, the extent to which such effects can be harnessed in real-world applications—characterized by complex or even extreme environments—remains unclear.

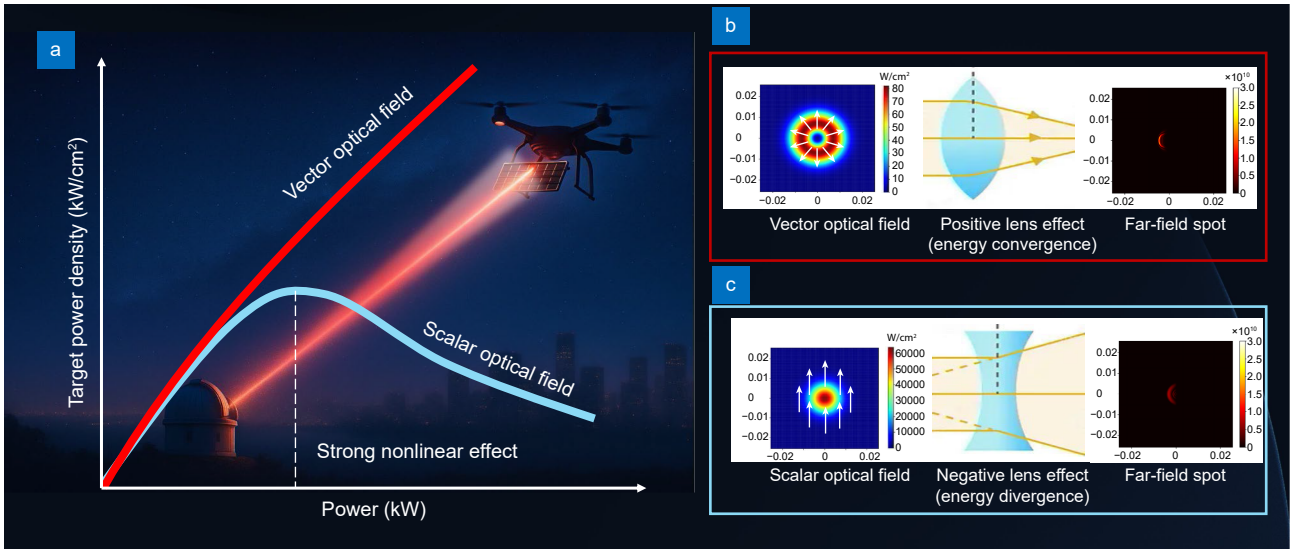

Fig. 5 | Surpassing the energy diffraction limit for power transfer. (**a**) Evolution of on-target power density with output power for high-power vector (red curve) and scalar (blue curve) lasers under strong nonlinear atmospheric effects. (**b**) Intensity distribution of the vector optical field (left panel); the positive atmospheric lens effect modulated by the vector optical field compensates for the thermal blooming-induced negative lens effect (middle panel); corresponding far-field laser spot (right panel). (**c**) Intensity distribution of the scalar optical field (left panel); the negative atmospheric lens effect modulated by the scalar optical field—driven by thermal blooming—causes energy divergence (middle panel); corresponding far-field laser spot (right panel).

Conclusion and perspectives

To date, cross-scale VOF manipulation has achieved over threefold improvements in both imaging resolution and power density for long-range optical applications. These findings provide direct evidence that the far-field diffraction limit of light—traditionally viewed as a fundamental barrier—can be overcome for both information and energy transfer. Cross-scale VOF manipulation is expected to play a pivotal role in remote optical imaging, laser communication, LWPT, and related fields. Several promising directions warrant further investigation:

Vectorial digitelligent optics enhanced long-distance sub-diffraction limited imaging. FP imaging holds strong potential for achieving high-resolution observation in space-based environments, where the absence of atmospheric turbulence enables near-ideal wavefront propagation. By integrating satellite constellations, array cameras, and lightweight onboard processing algorithms, real-time super-resolution imaging could become feasible for large-scale remote-sensing missions. Nevertheless, extending FP imaging to long-range and terrestrial applications remains challenging. The foremost difficulty lies in preserving wavefront phase accuracy over kilometer-scale paths, where atmospheric turbulence and thermal gradients induce non-stationary phase distortions that violate conventional FP assumptions. Photon scarcity and speckle decorrelation further constrain reconstruction quality at low signal-to-noise ratios, while existing phase-retrieval algorithms remain sensitive to partial coherence and temporal instability. Future advances will require adaptive optics for turbulence compensation, photon-efficient multiplexed acquisition, and physics-informed reconstruction algorithms, supported by compact and vibration-stable optomechanical architectures. Overcoming these challenges will be crucial for transitioning FP imaging from controlled laboratory environments to practical long-range systems.

For reflective LiDAR tomography, incorporating polarization information provides a promising route toward resolutions beyond those of conventional scalar systems. By combining single-photon detection with polarization-resolved measurements, one can jointly infer a target's motion state, surface composition, and structural anisotropy from its polarization signatures. Leveraging the polarization dimension thus introduces an additional degree of freedom to surpass traditional spatiotemporal detection limits and enhance target discrimination under complex scenes. Looking forward, reflective LiDAR tomography is expected to evolve into a distributed and intelligent sensing network. By synchronizing multiple LiDAR stations to achieve multi-view angular diversity, high-fidelity 3D reconstruction of non-

cooperative or dynamic targets can be realized without mechanical scanning. This approach paves the way for real-time tomography of extended or obscured objects such as space debris and partially shadowed satellites. Our recent demonstration of scanning-free non-line-of-sight (NLOS) imaging via LiDAR tomography at a 3.3 km stand-off distance—achieving centimeter-scale resolution within minutes—further verifies its feasibility. Future research will focus on high-throughput photon management under ultra-low return flux, temporal-preserving synchronization among distributed nodes, and robust inverse-model-based reconstruction algorithms resilient to turbulence and occlusion. Addressing these issues will be key to advancing LiDAR tomography from proof-of-concept experiments to practical, all-weather, and globally networked imaging infrastructures.

High-capacity and high-security laser communication. Vector optical beams offer a promising approach to realizing high-capacity, high-security, and turbulence-resilient FSO communication. Theoretically, their infinite set of orthogonal modes can be leveraged to substantially enhance FSO system channel capacity—an advantage that has attracted extensive research interest. Notably, the intrinsic vectorial nature of these beams remains largely intact during propagation through turbulent channels[57,58]. By harnessing this property, high-capacity, turbulence-resilient secure communication can be achieved via VOF manipulation[59,60]. Moreover, high-power VOFs can effectively counteract thermal blooming, leading to an enhanced photon energy density at the receiver and, consequently, improved tracking, pointing, and communication performance. These advantages could be particularly valuable for deep-space communication links.

High-power-resistant VOF device. Traditional vectorial optical field manipulation devices—such as spatial light modulators (SLMs)—suffer from large pixel sizes (typically ~8 μm) and low laser-induced damage thresholds (LIDT, typically 1–10 J/cm^2), hindering high-power VOF manipulation in long-range applications. Recent studies have shown that femtosecond laser-induced birefringent nanostructures embedded in silica glass can serve as building blocks for geometric phase elements with high optical efficiency and LIDT. Experimental results verify transmittance exceeding 99.4% in the near-infrared range and an LIDT as high as 68.0 J/cm^2 (at 1064 nm, 6 ns)[61]—providing a promising pathway for generating high-power VOFs.

Laser-induced atmosphere engineering. Although atmospheric turbulence is traditionally viewed as a detrimental factor in long-range optical propagation—inducing beam wander, scintillation, phase distortion, and image degradation—recent studies indicate that turbulence may not always function solely as a limiting factor. Instead, under carefully controlled conditions, it can be harnessed as a resource to surpass conventional diffraction limits and improve optical performance[62]. Among various techniques, VOF manipulation emerges as a powerful strategy to adaptively manipulate the spatial and temporal structure of optical fields. By tailoring the vectorial state of light, one can compensate for thermally induced negative lenses caused by high-power laser propagation—effectively increasing the beam quality and focusing performance.

References

1. Luo XG. Metasurface waves in digital optics. *J Phys Photonics* **2**, 041003 (2020).
2. Luo XG. Digital optics and optical intelligent agent. *Appl Phys Lett* **127**, 010501 (2025).
3. Ebbesen TW, Lezec HJ, Ghaemi HF et al. Extraordinary optical transmission through sub-wavelength hole arrays. *Nature* **391**, 667–669 (1998).
4. Pu M, Guo Y, Li X et al. Revisitation of extraordinary young's interference: from catenary optical fields to spin–orbit interaction in metasurfaces. *Acs Photonics* **5**, 3198–3204 (2018).
5. Luo XG. Principles of electromagnetic waves in metasurfaces. *Sci China Phys Mech Astron* **58**, 594201 (2015).
6. Luo XG. Engineering optics 2.0: a revolution in optical materials, devices, and systems. *ACS Photonics* **5**, 4724–4738 (2018).
7. Luo XG. *Engineering Optics 2.0: A Revolution in Optical Theories, Materials, Devices and Systems* (Springer, Singapore, 2019).
8. Luo XG. Subwavelength artificial structures: opening a new era for engineering optics. *Adv Mater* **31**, 1804680 (2019).
9. Choi Y, Yang TD, Fang-Yen C et al. Overcoming the diffraction limit using multiple light scattering in a highly disordered medium. *Phys Rev Lett* **107**, 023902 (2011).
10. Pu MB, Li X, Ma XL et al. Catenary optics for achromatic generation of perfect optical angular momentum. *Sci Adv* **1**, e1500396 (2015).
11. Luo XG, Pu MB, Zhang F et al. Vector optical field manipulation via structural functional materials: tutorial. *J Appl Phys* **131**, 181101 (2022).
12. Zhang F, Pu MB, Guo YH et al. Synthetic vector optical fields with spatial and temporal tunability. *Sci China Phys Mech Astron* **65**, 254211 (2022).
13. Zhang F, Guo YH, Pu MB et al. Meta-optics empowered vector visual cryptography for high security and rapid decryption. *Nat Commun* **14**, 1946 (2023).
14. Fan JX, Li ZL, Xue ZQ et al. Hybrid bound states in the continuum in terahertz metasurfaces. *Opto-Electron Sci* **2**, 230006 (2023).

15. He C, Antonello J, Booth MJ. Vectorial adaptive optics. *eLight* **3**, 23 (2023).
16. Sande SI, Deng YD, Bozhevolnyi SI et al. Spin-controlled generation of a complete polarization set with randomly-interleaved plasmonic metasurfaces. *Opto-Electron Adv* **7**, 240076 (2024).
17. Nan T, Zhao H, Guo JY et al. Generation of structured light beams with polarization variation along arbitrary spatial trajectories using tri-layer metasurfaces. *Opto-Electron Sci* **3**, 230052 (2024).
18. Jo Y, Park H, Yoon H et al. Advanced biological imaging techniques based on metasurfaces. *Opto-Electron Adv* **7**, 240122 (2024).
19. Liu XY, Zhang JC, Leng BR et al. Edge enhanced depth perception with binocular meta-lens. *Opto-Electron Sci* **3**, 230033 (2024).
20. Kang D, Heo H, Yang Y et al. Liquid crystal-integrated metasurfaces for an active photonic platform. *Opto-Electron Adv* **7**, 230216 (2024).
21. Li J, Lu XG, Li H et al. Racemic dielectric metasurfaces for arbitrary terahertz polarization rotation and wavefront manipulation. *Opto-Electron Adv* **7**, 240075 (2024).
22. Guo YH, Lei YS, Pu MB et al. Vectorial digitelligent optics for high-resolution non-line-of-sight imaging. *Engineering* **45**, 70–78 (2025).
23. Zhang F, Bao HL, Pu MB et al. Dispersion-engineered spin photonics based on folded-path metasurfaces. *Light Sci Appl* **14**, 198 (2025).
24. Xu T, Wang CT, Du CL et al. Plasmonic beam deflector. *Opt Express* **16**, 4753–4759 (2008).
25. Yu NF, Genevet P, Kats MA et al. Light propagation with phase discontinuities: generalized laws of reflection and refraction. *Science* **334**, 333–337 (2011).
26. Capasso F. The future and promise of flat optics: a personal perspective. *Nanophotonics* **7**, 953–957 (2018).
27. Luo XG. Multiscale optical field manipulation via planar digital optics. *ACS Photonics* **10**, 2116–2127 (2023).
28. Pu MB, Li X, Guo YH et al. Nanoapertures with ordered rotations: symmetry transformation and wide-angle flat lensing. *Opt Express* **25**, 31471–31477 (2017).
29. Guo YH, Ma XL, Pu MB et al. High-efficiency and wide-angle beam steering based on catenary optical fields in ultrathin metalens. *Adv Opt Mater* **6**, 1800592 (2018).
30. Zhang F, Pu MB, Li X et al. Extreme-angle silicon infrared optics enabled by streamlined surfaces. *Adv Mater* **33**, 2008157 (2021).
31. Luo XG, Ishihara T. Surface plasmon resonant interference nanolithography technique. *Appl Phys Lett* **84**, 4780–4782 (2004).
32. Luo XG. Plasmonic metalens for nanofabrication. *Nat Sci Rev* **5**, 137–138 (2018).
33. Liu L, Liu KP, Zhao ZY et al. Sub-diffraction demagnification imaging lithography by hyperlens with plasmonic reflector layer. *RSC Adv* **6**, 95973–95978 (2016).
34. Tang DL, Wang CT, Zhao ZY et al. Ultrabroadband superoscillatory lens composed by plasmonic metasurfaces for subdiffraction light focusing. *Laser Photonics Rev* **9**, 713–719 (2015).
35. Zhan Q. *Vectorial Optical Fields: Fundamentals and Applications* (World Scientific, 2013).
36. Pu MB, Ma XL, Guo YH et al. Theory of microscopic meta-surface waves based on catenary optical fields and dispersion. *Opt Express* **26**, 19555–19562 (2018).
37. Edrei E, Scarcelli G. Optical focusing beyond the diffraction limit via vortex-assisted transient microlenses. *ACS Photonics* **7**, 914–918 (2020).
38. Harrison J, Naidoo D, Forbes A et al. Progress in high-power and high-intensity structured light. *Adv Phys X* **9**, 2327453 (2024).
39. Smith DC. High-power laser propagation: thermal blooming. *Proc IEEE* **65**, 1679–1714 (1977).
40. Zhang SH, Wang AY, Xu JH et al. FPM-WSI: Fourier ptychographic whole slide imaging via feature-domain backdiffraction. *Optica* **11**, 634–646 (2024).
41. Xu FN, Wu ZP, Tan C et al. Fourier ptychographic microscopy 10 years on: a review. *Cells* **13**, 324 (2024).
42. Zhou R, Guo YH, Zhang Q et al. TurbFPNet: neural far-field turbulent Fourier ptychography with a camera array. *Optica* **12**, 1068–1078 (2025).
43. Wang R, Zhao Q, Loetgering L et al. Ptychography at all wavelengths. *Nat Rev Methods Primers* **5**, 69 (2025).
44. Zhang Q, Lu YR, Guo YH et al. 200 mm optical synthetic aperture imaging over 120 meters distance via macroscopic Fourier ptychography. *Opt Express* **32**, 44252–44264 (2024).
45. Dong SY, Horstmeyer R, Shiradkar R et al. Aperture-scanning Fourier ptychography for 3D refocusing and super-resolution macroscopic imaging. *Opt Express* **22**, 13586–13599 (2014).
46. Holloway J, Asif MS, Sharma MK et al. Toward long-distance subdiffraction imaging using coherent camera arrays. *IEEE Trans Comput Imaging* **2**, 251–265 (2016).
47. Holloway J, Wu YC, Sharma MK et al. SAVI: synthetic apertures for long-range, subdiffraction-limited visible imaging using Fourier ptychography. *Sci Adv* **3**, e1602564 (2017).
48. Li S, Wang BW, Liang KY et al. Far-field synthetic aperture Imaging via Fourier ptychography with quasi-plane wave illumination. *Adv Photonics Res* **4**, 2300180 (2023).
49. Tian ZM, Zhao M, Yang D et al. Optical remote imaging via Fourier ptychography. *Photon Res* **11**, 2072–2083 (2023).
50. Parker JK, Craig EB, Klick DI et al. Reflective tomography: images from range-resolved laser radar measurements. *Appl Opt* **27**, 2642–2643 (1988).
51. Knight FK, Klick D, Ryan-Howard DP et al. Laser radar reflective tomography utilizing a streak camera for precise range resolution. *Appl Opt* **28**, 2196–2198 (1989).
52. Li ZP, Ye JT, Ye WL et al. Single-photon laser reflective tomography over 7 km. *Opt Lett* **50**, 2970–2973 (2025).
53. Zhang XY, Shan LQ, Fang JJ et al. Super-resolution imaging using reflective tomography LiDAR over 10 km. *Adv Imaging* **2**, 051002 (2025).
54. Rubenchik AM, Fedoruk MP, Turitsyn SK. Laser beam self-focusing in the atmosphere. *Phys Rev Lett* **102**, 233902 (2009).
55. Helle MH, DiComo G, Gregory S et al. Beating optical-turbulence limits using high-peak-power lasers. *Phys Rev Appl* **12**, 054043 (2019).
56. DiComo G, Helle M, Kaganovich D et al. Nonlinear self-channeling of high-power lasers through controlled atmospheric turbulence. *J Opt Soc Am B* **37**, 797–803 (2020).
57. Zhu ZY, Janasik M, Fyffe A et al. Compensation-free high-dimensional free-space optical communication using turbulence-resilient vector beams. *Nat Commun* **12**, 1666 (2021).
58. Nape I, Singh K, Klug A et al. Revealing the invariance of vectorial structured light in complex media. *Nat Photonics* **16**,

538–546 (2022).
59. Song Z, Zhang YQ, Xu MF et al. High capacity turbulence-resilient free-space chaotic optical communication based on vector optical field manipulation. *J Lightwave Technol* **42**, 8647–8654 (2024).
60. Zhang Z, Li GY, Liu YL et al. Robust measurement of orbital angular momentum of a partially coherent vortex beam under amplitude and phase perturbations. *Opto-Electron Sci* **3**, 240001 (2024).
61. Wang QS, Fang Y, Meng Y et al. Vortex-field enhancement through high-threshold geometric metasurface. *Opto-Electron Adv* **7**, 240112 (2024).
62. Liu LC, Wu C, Li W et al. Active optical intensity interferometry. *Phys Rev Lett* **134**, 180201 (2025).

Acknowledgements

This work was supported by Temporal-spatial manipulation Infrastructure for vector Fields in Optics-Test Facility (TIFO-TF), and the National Natural Science Foundation of China (U24A6010, 62222513).

Author contributions

Y.-H. G., M.-B. P., and Y. L. performed the simulations and experiments. Y.-H. G., M.-B. P., Y. L., and M.-F. X. wrote the manuscript. All authors discussed and analyzed the data and results. M.-B. P. and X.-G. L. co-supervised the project.

Competing interests

Mingbo Pu and Xiangang Luo serve as the Editors for the Journal, and no other author has reported any competing interests.

Supplementary information

Supplementary information for this paper is available at https://doi.org/10.29026/oea.2025.250256

Scan for Article PDF